



<https://doi.org/10.36023/ujrs.2023.10.1.226>

UDC 528.88

## Modeling of radar scattering by aeolian desert landforms

A. Ya. Matveev, S. A. Velichko\*, D. M. Bychkov, V. K. Ivanov, V. N. Tsymbal

O. Ya. Usikov Institute for Radiophysics and Electronics of the National Academy of Sciences of Ukraine, 61085 Kharkiv, Ukraine

In order to identify the origin of the effect of anomalously narrowly-directional backscattering of radio waves (ANDBR) of the X-band in desert areas, the work describes a complex analysis of many years of research in the Sahara desert regions. According to the results of the analysis, which was carried out using the SAR radar data of the Envisat-1 satellite, results of contact measurements, weather conditions and taking into account modern theories, the characteristics of the scattering of radio waves by the aeolian landforms of the desert were modeled. A new model of anomalous backscatter is proposed, according to which the main scatterer towards the radar is a grid formed by the wind from electrified saltons and reptons at a height of 2–3 cm from the surface and repeating the landform of ripples and barchans. The new model made it possible to explain the main features of experimental studies of the ANDBR effect. Namely: the dependence of the normalized radar cross-section (NRCS) of the researched terrain on the near-surface wind speed up to 10 m/s with opposite directions of the wind and radar survey vectors, as well as with their mutual azimuthal deviation of  $\pm 45$  degrees. By using the new model, satellite monitoring of the near-surface layer moisture of the Earth desert regions at 3 cm and 5.6 cm radio wave length with radar viewing angles 30...35° is proposed.

**Keywords:** radar remote sensing, desert monitoring, anomalously narrowly-directional backscattering, sand electrified layer.

© A. Ya. Matveev, S. A. Velichko, D. M. Bychkov, V. K. Ivanov, V. N. Tsymbal. 2023

### 1. Introduction

Deserts occupy one fifth of the Earth's land and have a significant impact on the planet's climate. Aeolian processes in deserts lift millions of tons of sand, dust and various bacteria into the atmosphere and transport them over long distances, which complicates air and land transportation, and also affects human health (Lancaster, 2009; Schmidt et al., 1998; Ozer, 2006). These processes lead to desertification of nearby territories (Zolotokrylin, 2003) and constantly change the landscape of the deserts themselves. The latter means the creation of various structures on their surface in the form of, for example, sand ripples, dunes and barchans. The study of the processes of formation and extension of these structures makes it possible to assess the scale of the damage done and minimize its consequences.

To date, a wide range of experimental and theoretical works has been carried out to study the nature of the formation of such structures and the transport of dust-sand mixture into the atmosphere under the influence of wind (Kok et al., 2012; Kok et al., 2008; Stow, 1969; Namikas, 2003; Greeley et al., 1996; Schmidt et al., 1998; Malinovskaya, 2019). Methods for remote satellite monitoring of these phenomena have also been developed (Herrmann et al., 1999; Middleton et al., 2001; Ivanov et al., 2015a; Ivanov et al., 2015b; Ivanov et al., 2016; Ivanov, 2018; Bychkov et al., 2020a; Bychkov et al., 2020b; McHone et al., 1996; Stephen et al., 2005).

Multizone optical systems commonly used for monitoring make it possible to detect areas of dust formation only in the daytime and under conditions of weak cloudiness (Herrmann et al., 1999; Middleton et al., 2001). The manifestation of the effects of anomalously narrowly-directional backscattering of radio waves (ANDBR) was first detected in 1983 on radar images (RI) of the desert regions of the Sahara. These RI were obtained by using the Cosmos-1500 side-looking real-aperture (SLRAR) X-band satellite radar. The studies were continued using the Sich-1 X-band SLRAR and the Envisat-1 S-band synthetic aperture radar images (Ivanov et al., 2015a; Ivanov et al., 2015b; Ivanov et al., 2016; Ivanov, 2018; Bychkov et al., 2020a; Bychkov et al., 2020b). In 1994, multi-frequency and multi-polarization studies of the Sahara regions were carried out using the C/X-SIR-C/X-SAR space radar laboratory on board the Shuttle Endeavor (McHone et al., 1996). They also showed a significant increase in the intensity of radar signals reflected from the lee slopes of barchans at an incidence angle of about 32°, which coincides with the average angle of repose of desert sands (Al-Hashemiet al., 2018).

At the same time, simulation of scattering from aeolian structures in the Sahara Desert, using Ku- and S-band scatterometer data (ESCAT, NSCAT, QSCAT, TRMM-PR) (Stephen et al., 2005) and direct measurements of the normalized radar cross-section (NRCS)  $\sigma^0$  (Williams et al., 2004), showed values  $\sigma^0$  lower by 6–10 dB compared to the data of RCS surveys in the same regions, performed using the Envisat-1 SAR, SLRAR Cosmos-1500 and Sich-1 (Ivanov et al., 2015a;

\*E-mail: [sergey19118@gmail.com](mailto:sergey19118@gmail.com)

Ivanov et al., 2015b; Ivanov et al., 2016; Ivanov, 2018; Bychkov et al., 2020a; Bychkov et al., 2020b). Such a discrepancy indicates insufficient knowledge of the nature of the radio waves scattering by the structures created by the wind on the desert surface.

Therefore, in this work, in order to clarify the nature of the observed ANDBR, modeling was performed based on the analysis of data from long-term (2004–2011) surveys of the desert regions of the Sahara (El-Juf, Akshar and Trarza) by the Envisat-1 space SAR (project with the European Space Agency ESA Id: 30193). Image processing was carried out using standard ESA programs. The work uses correlating data from experimental and theoretical studies of the formation of aeolian landforms on the desert surface, which made it possible to propose a new model of ANDBR.

## 2. Primary data for modeling

As primary data in this paper, we used the generalized results of processing and analysis of satellite radar images of the Amatlich erg near the village of Akzhuzht in Mauritania (Ivanov et al., 2015a; Ivanov et al., 2015b; Ivanov et al., 2016; Ivanov, 2018; Bychkov et al., 2020a; Bychkov et al., 2020b). As a result, the following regularities were determined in the observation and in the parameters of ANDBR:

a) ANDBR is confidently observed on the erg surface in the autumn-winter period, when the northeast wind blows regularly at a speed of 2-8 m/s (Fig. 1 a). At a wind speed of 1.5–2 m/s, an increase in the number of bright reflecting points is observed on the radar image in the area of the supposed ANDBR;

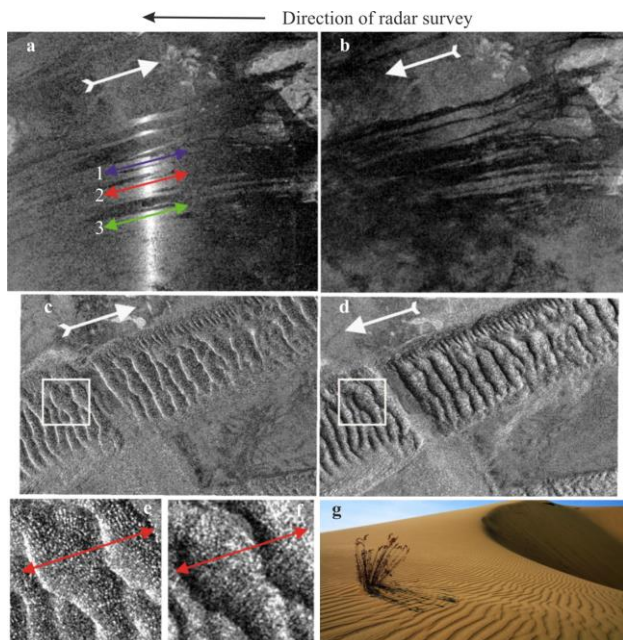


**Fig. 1.** The processing results of radar imaging Envisat-1 (Ivanov et al., 2015a; Ivanov et al., 2015b; Ivanov et al., 2016; Ivanov, 2018; Bychkov et al., 2020a; Bychkov et al., 2020b): ASA\_GM1\_1P20050112, ASA\_GM1\_1P20041226 of low-resolution (1000x1000 m, Fig. 1 a, b); ASA\_IMP\_1P20040421, ASA\_IMP\_1P200402126 of high resolution (25x25 m, Fig. 1 c, d); their fragments marked with white squares – Fig. 1 e, f (© ESA); Fig.1 g – optical image of barchans; the white arrows on the radar images indicate the direction of the wind

b) The cause of the ANDBR is the ridges of barchans, which intensely reflect radio waves when the radar survey is directed against the wind. The latter implies that the near-surface wind vector and the projection of the radar survey vector in the horizontal plane  $\vec{R}_{xy}$  are antiparallel ( $\vec{U}_{xy} \uparrow \downarrow \vec{R}_{xy}$ ). An example is presented in Fig. 1 a (bright stripes with  $\sigma_{\max}^o = +7$  dB) and Fig. 2 a. At the same time, with an increase in wind speed, an expansion of the signal backscatter pattern and signal amplitude saturation are observed.

In another typical case, the wind and survey direction smatch, which means that the vectors  $\vec{U}_{xy}$  and  $\vec{R}_{xy}$  are parallel ( $\vec{U}_{xy} \uparrow \downarrow \vec{R}_{xy}$ ). There at the barchans reflect radio signals significantly less (Fig. 1 b, dark stripes with  $\sigma_{\min}^o$  less than  $-20.4$  dB);

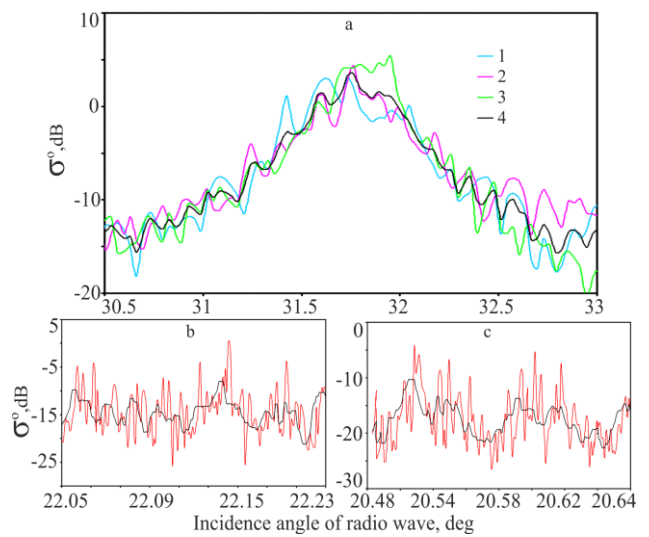


**Fig. 2.** Angular dependences  $\sigma^o$  (Fig. 2 a) in sections 1, 2, 3 of the radar image in Fig. 1 a (black curve – averaging over curves 1, 2, 3); Fig. 2 b and Fig. 2 c –  $\sigma^o$  in sections in Fig. 1 e, 1 f, respectively (black curve is the angular dependence after median filtering)

c) ANDBR is observed during radar survey in the X-band (SLRARCosmos-1500, Sich-1) at angles of incidence of radio waves  $\theta = 31.5...33^\circ$  and in the C-band at  $\theta = 32...34^\circ$  (SAR Envisat-1, Fig. 2 a) and varies within  $\Delta\sigma^o = 2...3$  dB when the wind direction changes in the azimuthal plane relative to the survey direction at angles  $\pm 45^\circ$ .

d) During radar survey at angles  $\theta \leq 25^\circ$  (Fig. 1 b...f), only single point scatterers on the crests of barchans reflect; as a result, with median filtering, the average  $\sigma_{med}^o$  along the line is  $\approx -13$  dB (Fig. 2 b) and  $\approx -17$  dB (Fig. 2 c)

It is important to note that the lee slopes of barchans and sand ripples form a certain angle with the underlying surface, which is the angle of repose of sand. For sand, it is equal to  $\psi = 30...34^\circ$  (Al-Hashemi et al., 2018) and depends only on its moisture content, sizes of its constituent particles, and gravitational force.

### 3. Modeling

Before modeling, let us briefly outline the current state of the physics of the aeolian forms formation in deserts (Lancaster, 2009; Schmidt et al., 1998; Ozer, 2006; Zolotokrylin, 2003; Kok et al., 2012; Kok et al., 2008; Stow, 1969; Namikas, 2003; Greeley et al., 1996; Schmidt et al., 1998; Malinovskaya, 2019). Under the action of the near-surface wind, dust and sand particles, depending on their size, can move and roll over the surface, and when a certain speed is reached, break away from it, making bounces (saltating). In the air, particles experience turbulent wind pulsations that change the length of their bounces. Hitting the surface after the bounces, the primary particles (saltons) knock out secondary, tertiary, etc. particles from it (reptons). Different lengths of bounces create inhomogeneities on the surface, forming a landform first of ripples, and then of barchans. Previously, it was considered (Lancaster, 2009; Ivanov et al., 2015b) that due to the difference in wind pressures at the top of the barchan and at its base, a vortex of electrically charged particles is created on the leeward slope of the barchan. But, when radio waves are scattered on a narrow part of the surface of the “cylinder” created by the vortex, the effective scattering value towards the radar is comparable to the SAR noise equivalent ( $\sim -20$  dB). Recent estimates (Malinovskaya, 2019) have shown that the energy of such a vortex is only enough for the collapse of particles from the top of the barchan. Therefore, saltons and reptons can bounce over the ridge, knocking out only reptons from the leeward slope. In addition, the bounce length of saltons and reptons also depends on their mass and the electrification of particles, which acquire a negative charge upon separation from the surface and due to collisions with charged particles and dust. With an increase in the number of charged particles raised into the air, the electric field intensifies in the near-surface layer. This leads to a limitation of the particle bounce amplitude and actually creates a layer of negatively charged particles and dust at a height of 2–3 cm (Kok et al., 2008; Namikas, 2003; Greeley et al., 1996; Ivanov et al., 2015b), which repeats the shape of the inhomogeneity growing on the surface. The normalized radar cross-section of this layer, according to Envisat-1 SAR data, is very close to the values obtained by measuring the angular scattering pattern of radio waves of the same range by an ionized particle flux in fluorescent lamps (Bychkov et al., 2020a; Bychkov et al., 2020b; Tajudin, 2014). Since ionization processes are observed only in liquids and gases, for an electrified sand-dust layer with similar scattering characteristics, we will further use the term “electrified” layer.

As far as, in the absence of wind, sand reflects radio waves much less (Ivanov et al., 2016; Stephen et al., 2005), while the wind contributes to the appearance of electrically charged saltons and reptons, we will find out by means of simulation which processes are responsible for the experimentally observed intense ANDBR.

Obviously, the observed backscattering of radio waves can occur:

$$\begin{aligned} ma_x &= -\frac{\pi D_p^2}{8} \rho_a C_d |V_R| (U - v_x) \\ ma_z &= \frac{\pi D_p^2}{8} \rho_a \left[ -C_d |V_R| v_z + C_1 (U_{top}^2 - U_{bot}^2) \right] - mg + qE, \end{aligned} \quad (1)$$

where  $m$  and  $D_p$  are the mass and diameter,  $q$  is the charge of a particle moving with accelerations  $a_x$  and  $a_z$  in the horizontal and vertical directions,  $v_x$  and  $v_z$  are the corresponding particle velocities. In this case,  $V_R$  is the vector of the difference between the velocities of the particle and the wind;  $U$  is the horizontal wind speed at the location of the particle,  $U_{top}$  and  $U_{bot}$  are the wind speeds above and below the particle,  $E$  is the electric field at the location of the particle,  $\rho_a$  is the air density;  $g$  is the gravitational constant.  $C_d$  is the particle shape drag coefficient in laminar flow,  $C_1$  is the particle lift coefficient due to the Magnus effect.

Let us first transform the system of equations (1), considering the particles to be spherical and excluding the mass of particles through the relation  $m = \pi D_p^3 / \rho_s$ , where  $\rho_s$  is the density of quartz. Next, we replace the acceleration values with the time derivatives of the velocity components. As a result, we get:

a) or on negatively charged saltons and reptons on the descending segments of their motion trajectories above the barchans surface;

b) or on an electrified layer of saltating particles repeating the shape of barchans sand ripples.

To clarify this, it is necessary to perform numerical simulation of the trajectories of the movement of electrified sand particles near the surface under the influence of wind, i.e. during saltation.

The simulation was carried out using the equations of motion given in (Schmidt et al., 1998; Kok et al., 2008). The initial form of the system of equations for the two-dimensional case:

$$\begin{aligned} \frac{\partial v_x}{\partial t} &= \frac{3}{4} \frac{\rho_a}{D_p \rho_s} C_d |V_R| (U - v_x) \\ \frac{\partial v_z}{\partial t} &= \frac{3}{4} \frac{\rho_a}{D_p \rho_s} \left[ -C_d |V_R| v_z + C_1 (U_{top}^2 - U_{bot}^2) \right] - g + \frac{q}{m} E. \end{aligned} \quad (2)$$

Note that only the particle diameter  $D_p$  and the charge-to-mass ratio, which we denote below as  $q/m = Q_m$ , remain as parameters of the particle.

The dependences of the horizontal wind speed and electric field strength on the height above the surface are essentially non-linear. So, for the dependence  $E(z)$  based on the experimental data (Schmidt et al., 1998), we use the relation:

$$E(z) = E_{max} z^{-\beta}, \quad (3)$$

where  $E_{max}$  is the maximum electric field strength measured at a height of  $z = 1$  cm.

The logarithmic profile of the wind speed over a rough surface in the case of a laminar flow is described as (Prandtl, 1935):

$$U(z) = \frac{u^*}{k} \ln \left( \frac{z}{z_0} \right), \quad (4)$$

where  $k = 0.4$  is the Karman's constant,  $u^*$  is the friction velocity, determined at the level  $z_0$ -characteristic surface roughness.

One of the features of the current modeling is taking into account the surface profile, namely the presence of sand ripples and barchans. To take into account the latter, the function of a triangular-asymmetric wave of the general form is used.

$$h(x) = H(L_{BR}, \alpha_1, \alpha_2), \quad (5)$$

where  $L_{BR}$  is the period or horizontal scale of the considered horizontal inhomogeneities, and  $\alpha_1, \alpha_2$  are the angles of the windward and leeward slopes of the barchan or ripple, respectively. In this case, to determine the profiles of the horizontal wind speed and electric field strength, the following relations are used:

$$z_{hU} = (z - h(x)) \left( \frac{U}{u^*} \right)^{\beta}; \quad z_{hE} = (z - h(x)), \quad (6)$$

where  $\vec{n}_h(x)$  is the normal to the surface at the point with coordinate  $x$ .

Taking into account the above relations, we represent the system of equations (2) in the form

$$\begin{aligned} \frac{\partial v_x}{\partial t} &= F_x(t, x, z, v_x, v_z); & \frac{\partial x}{\partial t} &= v_x \\ \frac{\partial v_z}{\partial t} &= F_z(t, x, z, v_x, v_z); & \frac{\partial z}{\partial t} &= v_z, \end{aligned} \quad (7)$$

where  $F_x, F_z$  are functionals built on the basis of the system of equations (2) and dependencies (3)–(6). For the numerical solution of the equations of motion, the symplectic Euler method is used as applied to the motion of a particle in two-dimensional space

$$\begin{aligned} v_{x(n+1)} &= v_{x(n)} + F_x(t_n, x_n, z_n) \Delta t \\ x_{(n+1)} &= x_n + v_{x(n+1)} \Delta t \\ v_{z(n+1)} &= v_{z(n)} + F_z(t_n, x_n, z_n) \Delta t \\ z_{(n+1)} &= z_n + v_{z(n+1)} \Delta t \end{aligned} \quad (8)$$

with the parameters considered below.

### 3.1. Parameters used in simulation

The particle sizes were chosen taking into account the experimental data on the distribution of diameters  $D_p$  both for the initial soil (sand) and for salting particles (Namikas, 2003). The results of these measurements and the electric field strength above the surface, created by the corresponding salting particles, are shown in Fig. 3.

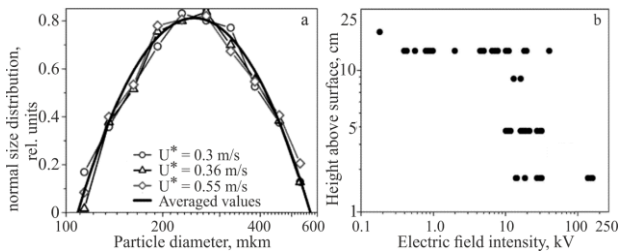


**Fig. 3.** Relative size distribution of sand particles (a) (Namikas, 2003) and electric field strength over the surface, created by salting particles (b) (Schmidt et al., 1998)

It can be seen from Fig. 3 a that the distribution of particle diameters is quasi-normal with a peak value of 250  $\mu m$  and an approximate size range from 100  $\mu m$  to 500  $\mu m$ . Therefore, modeling the motion of particles with diameters in this range should satisfactorily take into consideration the entire range of their sizes. The electric charge of the particles was taken into account

through the charge-to-mass ratio  $Q_m$ . According to (Schmidt et al., 1998), this value is in the range from  $-60$  to  $60 \mu C/kg$ . The profile of the electric field strength given by dependence (3) is characterized, first of all, by the maximum value  $E_{max}$ , which can be estimated from (Namikas, 2003) (Fig. 3 b). At a height of 1 cm, this value ranges from 20 to 200 kV/m. The exponent in the vertical profile of the electric field, according to the approximation (Schmidt et al., 1998)  $\beta = -0.6$ , the friction velocity  $u^*$  changed in the simulation from 0.1 to 1.0 m/s. To determine the wind speed profile in height, according to (4), the characteristic surface roughness was assumed to be  $z_0 = 0.002$  m, based on profile  $U(z)$  calculations at various friction velocities  $u^*$  and ratios  $U(z)/u^*$ . The particle shape drag coefficient was considered equal to  $C_d = 0.47$ , as for a smooth sphere in a laminar flow (at Reynolds number  $Re < 10^5$ ). Particle lifting coefficient  $C_l = 0.85 C_d$  (Kok et al., 2008). Rebound speed, i.e. the initial vertical velocity of the particle at the moment  $t = 0$  in the iterative scheme (8) varied within  $v_{z(t=0)} = 0.4 - 0.8$  m/s (Schmidt et al., 1998). When modeling the profile of the underlying surface, the periods of inhomogeneities were chosen as  $L_R = 0.15$  m and  $L_B = 15$  m for sand ripples and barchans, respectively. The slope angles of the barchans sand ripples were set as follows: the angle of the windward slope  $\alpha_1 = 10...15^\circ$  (Malinovskaya, 2019; Pye et al., 2009) and the angle of the leeward slope  $\alpha_2 = 30...34^\circ$  (Al-Hashemi et al., 2018; Pye et al., 2009).

### 3.2 Simulation results

Paragraphs 3a, 3b list two possible cases of ANDBR occurrence.

In the 1st case, it is assumed that the observation of ANDBR takes place on the descending segments of the trajectory of electrically charged saltions and reptons. In this instance, the descending segments of the trajectories of these particles should form a grating capable of effectively scattering of 3 cm and 5.6 cm radio waves towards the radar.

To verify this, we simulate the trajectories and their angles of inclination by solving the system of equations (7). Calculations were performed for various values of the parameters specified in paragraph 3.1. Figure 4, as an example, presents the simulation results for the following parameters: particle rebound velocity  $v_{z(t=0)} = 0.8$  m/s, particle size  $D_p = 100-500 \mu m$ , friction velocity  $u^* = 0.4$  m/s, charge to mass ratio  $Q_m = -60 \mu C/kg$ , maximum electric field strength  $E_{max}(z) = 100$  kV/m. Figures 4 a and 4 b show that the trajectories of saltions and reptons over the windward and leeward slopes cannot create the necessary quasi-periodic structure over their surface. This is due to the fact that the length of bounces of saltating particles depends on their size (Fig. 4 a), electric field strength, near-surface wind speed, etc. (Fig. 4 b). In support of this, Fig. 4 c presents the calculated angular dependences of the trajectories of motion of the specified set of particles over the barchan. These dependences demonstrate the absence of any angular selectivity of specular backscattering of radio waves in all parts of the trajectories.

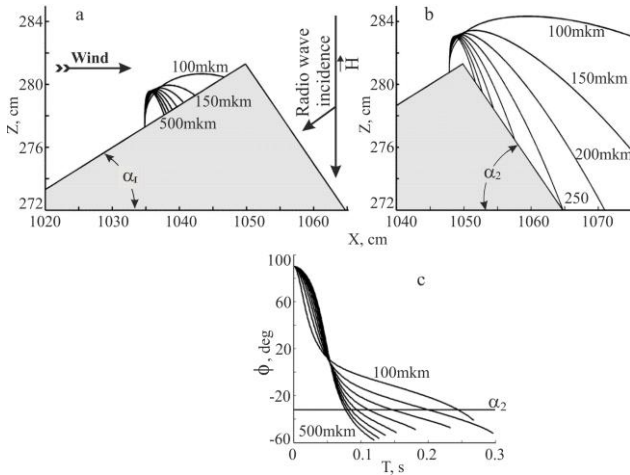


**Fig. 4.** Examples of calculated motion trajectories (a, b) and their inclination angles (c)

$\varphi = \arctan(v_z/v_x)$  of saltating particles with a size of 100–500  $\mu\text{m}$  along the windward (a) and leeward (b) slopes of the barchan.  $\vec{H}$  – normal vector from flight path to nadir track

In the 2nd case (see paragraph 3b), we assume that the occurrence of the ANDBR is possible on an electrified layer of salting particles repeating the shape of the barchan and ripples.

Recall that in (Ivanov et al., 2015b) it was concluded that the electric fields arising during the aeolian transport of sand are sufficient to create electrization of saltating sand and air particles in a narrow near-surface layer (paragraph 3b). This layer repeats the shape of the sand ripple and creates on its leeward slope a system of reflective electrified quasi-flat areas – reflectors (facets) responsible for the formation of ANDBR under the condition of the opposite direction of the wind vector and radar observation. Taking into account the present data (Malinovskaya, 2019) on the processes on the leeward slope of the barchan, it is appropriate to assume that sand particles, salting over the surfaces of the windward and leeward slopes of the barchan, also form a total electrified layer above it (Fig. 5). The saltating particles, bending around the surface of the windward slope of the barchans (Fig. 4 b), bounce over the surface of the leeward layer and create an electrified layer on its leeward slope for additional reflection of radio waves (Fig. 5). The total contribution of a barchans with ripples to the ANDBR depends on their geometry and size. The shape of a single barchans has a crescent shape, the horns of which are directed along the wind propagation. The horns size depends on the complex conditions for the formation of the entire barchans ridge (Fig. 1 c...f). The height of the barchan in various deserts can range from 2–3 m to 2–30 m or more; the ripple wavelength is from 0.5 to 25 cm, the typical ripple height is 0.5–5 cm (Malinovskaya, 2019; Stephen et al., 2005; Bagnold, 1941). The contribution of barchan backscattering to ANDBR, according to our estimates, is  $\sim 55\text{...}65\%$ , depending on the ratio of the heights of the barchans and the ripples that repeat the shape of the barchan surface (Fig. 5). At the same time, we recall that the lee slopes of barchans and ripples make an angle with the underlying surface, which is the angle of repose of sand  $\psi = 30\text{...}34^\circ$  (Al-Hashemi et al. 2018). And when radio waves are

scattered from leeward slopes at an angle  $90^\circ$  towards the radar, the sand repose and radio wave incidence angles are equal  $\alpha_2 = \alpha_r$  (Fig. 5 b).

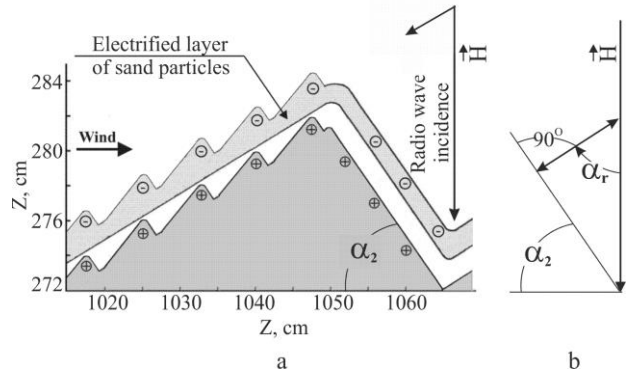


**Fig. 5.** Formation of the cumulative near-surface layer of electrically charged saltating sand particles over the upper part of the barchans (a); the geometry of the relationship between the repose angle  $\alpha_2$  and the angle of radio wave incidence  $\alpha_r$  (b).  $\vec{H}$  – normal vector from flight path to nadir track

As a result of the simulation, we have proposed the model of combined facet backscattering (MCFB), which is the sum  $\sigma_\Sigma$  of the received radar signals:

$$\sigma_\Sigma = \sum_1^m \sigma_{\text{ELB}} + \sum_1^n \sigma_{\text{ELR}}, \quad (9)$$

where  $\sigma_{\text{ELB}}$  and  $\sigma_{\text{ELR}}$  are the radar cross-sections of the sum of electrified layers repeating the lee slopes of barchans and ripples, respectively:  $m$  and  $n$  are the numbers of scattering slopes of barchans sand ripples within the resolution element on the surface.

To confirm the simulation results within the framework of the proposed model, we compare them with the experimental data obtained (see paragraphs 2a...2d).

### 3.3. Mutual analysis of experimental data and simulation results

1. The observed effect of a significant increase in the total brightness of the radar image of the surface of barchans and ripples with an increase in wind speed (paragraphs 2a, b) is confirmed by modeling the backscattering of radio waves by an electrified layer of sand-dust mixture above the surface, formed by facets of ripples and barchans. As the wind speed increases, the density of the near-surface layer of charged particles grows, which leads to an increase in the backscattering of radio waves towards the radar. In addition, with an increase in the near-surface wind speed to 8–10 m/s, saturation of the scattered signal received by the radar is experimentally observed (Fig. 6 b). Hence, it can be assumed that a further increase in wind speed will lead to the appearance of high-energy saltans and reptons, which destroy the electrified layer above the surface of barchans covered with ripples. This is a prerequisite for the beginning of a sandstorm. The values of backscattering coefficients of barchan and ripple leeward facets, obtained earlier (Ivanov et al., 2016) without taking into account the electrization of sand, are less than those observed by 1–2 orders of magnitude.

2. The effect of radio wave scattering by an electrified layer over the aeolian form surfaces was used by us in the proposed model to explain the ANDBR observed on radar images of different radio wavelength bands (paragraph 2c). With opposite directions of the wind and radar survey, the total electrified layer keeps the slope angles of the lee facets practically unchanged during the SAR survey. This confirms the faceted mechanism of backscattering of radio waves proposed in the model, because the angle of the lee slopes of ripples and barchans with the underlying surface is optimal for experimental observation of the ANDBR and coincides with the angle of repose of sand, which is independent of the radio wavelength band.

3. The model also explains minor variations  $\sigma^{\circ}$  when the wind direction changes at angles  $\pm 45^{\circ}$  in the azimuthal plane relative to the radar survey vector (paragraph 2c). On Fig. 1 f, 1 g, it can be seen that the lee slope of the barchans has a crescent shape with a constant slope angle. At the same time, the wind forms the direction of the ripples facets on the surface of the windward slope, also repeating the crescent shape. This results in a weak azimuthal dependence of  $\sigma^{\circ}$ .

4. With coinciding directions of wind and radio survey (paragraph 2d) or opposite directions, but at angles of incidence less than the repose angle, the windward and leeward slopes create a reflection like ordinary sand with  $\sigma^{\circ} \leq -10$  dB (Fig. 2 a and 2 b, c).

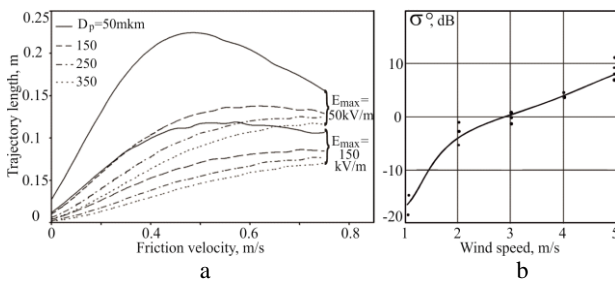


**Fig. 6.** Calculated lengths of trajectories of saltating particles on the windward slope depending on the friction velocity (a), experimental dependences of the NRCS at ANDBR on the wind speed (b) (Bychkov et al., 2020b)

It is also necessary to note the characteristic features found when calculating the dependences of the lengths of the particle transfer trajectories on the wind speed (Fig. 6 a) based on the simulation results. The lengths of the transfer trajectories increase as the friction velocity changes from 0 m/s to 0.45–0.6 m/s, then decrease. This may be due to the fact that as the wind speed increases, the particle trajectories become more flat, i.e., the particles pass at a height where the electric field strength is much higher (Fig. 3 b). This also agrees qualitatively with the results of (Namikas, 2003; Ho et al., 2014), which correlates with the explanations for the saturation of the ANDBR level when the wind speed increases above certain values (Fig. 6 b).

#### 4. Conclusions

In this paper, in order to explain the nature of the experimentally observed effect of anomalously narrowly-directional backscattering of radio waves

(ANDBR), studies were carried out on a complex analysis of long-term Envisat-1 SAR radar surveys of the Sahara desert regions using contact and meteorological data. The characteristic features of the manifestation of ANDBR on radar images of the SAR Envisat-1 are modeled and explained.

According to the simulation results:

1) as a result of research, a model of combined facet backscattering (MCFB) on a near-surface electrified layer was proposed and analyzed. The layer is created by electrically charged sand particles, arises under the action of the wind and repeats the shape of the ripples and the barchan itself. The main scatterers of radio waves (facets) towards the radar are the inhomogeneities of the electrified layer formed over the lee slopes of ripples and barchans;

2) the proposed model made it possible to explain the increase in RCS with a growth in the near-surface wind speed up to 10 m/s and opposite vectors directions of the wind speed and radar sensing of the surface. Also, this explains the RCS variations with the mutual azimuthal deviation of these vectors by  $\pm 45$  deg. The results obtained can be used to warn about the onset of dust storms.

3) since the angles of the lee slopes of ripples and barchans (repose angles) are practically unchanged with a fixed distribution of natural sizes of sand particles (50–500  $\mu\text{m}$ ) and sand moisture, this feature can be used to control the moisture content of the near-surface layer in desert areas. This is possible from measurements of the ANDBR angle using satellite surveys at radio wavelengths of 3 cm and 5.6 cm, including viewing angles 30...35°.

4) to test the combined model for radar monitoring of desert areas of the Earth's surface at longer radio waves, additional studies are needed.

#### References

- Al-Hashemi, H. M. B., & Al-Amoudi, O. S. B. (2018). A review on the angle of repose of granular materials. *Powder Technology*, 330, 397–417. DOI: <https://doi.org/10.1016/j.powtec.2018.02.003>.
- Bagnold, R. A. (1941). *The Physics of Blown Sand and Desert Dunes*. London, U.K.: Methuen.
- Bychkov, D. M., Ivanov, V. K., Matveyev, A. Ya., Tsymbal, V. N., & Yatsevich, S. Ye. (2020a). Space-borne radar observation of near-surface wind effect on anomalously highly-directional backscattering of radio waves from aeolian processes of sand and dust transporting in desert regions. *Radiofiz. elektron.*, 25(1), 21–27. DOI: <https://10.15407/rej2020.01.021>.
- Bychkov, D. M., Ivanov, V. K., Matveyev, A. Ya., Tsymbal, V. N., & Yatsevich, S. Ye. (2020b). Space-borne radar observation of near-surface wind effect on anomalously highly-directional backscattering of radio waves from Aeolian processes of sand and dust transporting in desert regions. *Ukrainian Journal of Remote Sensing*, 24, 4–8. DOI: 10.36023/ujrs.2020.24.162.
- Greeley, R., Blumberg, D. G., & Williams, S. H. (1996). Field Measurements of the Flux and Speed of Wind-Blown Sand. *Sedimentology*, 43, 41–52.
- Herrmann, L., Stahr, K., & Jahn, R. (1999). The Importance of Source Region Identification and Their Properties for Soil-Derived Dust: the Case of Harmattan Dust Sources for Eastern West Africa. *Contributions to Atmospheric Physics*, 72, 141–150.

- Ho, T. D., Valance, A., Dupont, P., & Ould El Moctar, A. (2014). Aeolian sand transport: Length and height distributions of saltation trajectories. *Aeolian Research*, 12, 65–74.
- Ivanov, V. K. (Eds.) (2018). *Radar monitoring of natural and anthropogenic hazardous phenomena*. (Part 2). Lambert Academic Publishing, Germany. Retrieved from <https://www.lapublishing.com>.
- Ivanov, V. K., Matveev, A. Ya., Tsymbal, V. N., & Yatsevich, S. Ye. (2015a). Radar investigations of the aeolian sand and dust transporting manifestations in desert areas. *Telecommun. Radio Eng.*, 74(14), 1269–1283.
- Ivanov, V. K., Matveev, A. Ya., Tsymbal, V. N., & Yatsevich, S. Ye. (2015b). Radar monitoring of aeolian sand and dust transporting manifestations in desert areas. *Fiz. Osnovy Priborostr.*, 4(4), 46–59.
- Ivanov, V. K., Matveev, A. Ya., Tsymbal, V. N., Yatsevich, S. Ye., & Bychkov, D. M. (2016). Spaceborne radar identification of desert regions as suppliers of dust into the atmosphere. *Ukrainian Journal of Remote Sensing*, 11, 39–47. Retrieved from <https://ujrs.org.ua/ujrs/article/view/87/pdf>.
- Kok, J. F., Parteli, E. J. R., Michaels, T. I., & Bou Karam, D. (2012). The Physics of Wind-Blown Sand and Dust. *Reports on Progress in Physics*, 75, 106901.
- Kok, J. F., & Renno, N. O. (2008). Electrostatics in wind-blown sand. *Physical Review Letters*, 100, 014501. DOI: 10.1103/PhysRevLett.100.014501.
- Lancaster, N. (2009). Aeolian Features and Processes. In Young, R. & Norby, L. *Geological Monitoring*, 1–25, Boulder, Colorado, Geological Society of America, DOI: 10.1130/2009.monitoring(01).
- Malinovskaya, E. A. (2019). Transformation of aeolian relief forms under wind influence. *Izvestiya RAN, Atmospheric and Oceanic Physics*, 53(1), 54–64.
- McHone, J. F., Greely, R., & Blumberg, D. (1996). SIR-C/X-SAR Radar Studies; Impact and Aeolian Features, Borkov Region Northern Chad. *Lunar and Planetary Science*, 27, 849. Retrieved from <http://adsabs.harvard.edu/full/1996LPI...27..849M>.
- Middleton, N. J., & Goudie, A. S. (2001). Saharan dust: Sources and trajectories. *Transactions of the Institute of British Geographers*, 26(2), 165. DOI:10.1111/1475.
- Namikas, S. L. (2003). Field Measurement and Numerical Modeling of Aeolian Mass-Flux Distributions on a Sandy Beach. *Sedimentology*, 50, 303–326.
- Ozer, P. (2006). *Dust in the Wind and Public Health: Example From Mauritania*. International Conference Desertification, Migration, Health, Remediation and Local Governance. Royal Academy for Overseas Sciences United Nations Brussels. 55–74.
- Prandtl, L. (1935). The mechanics of viscous fluids. *Aerodynamic Theory*, III(G), 34, Berlin: Springer.
- Pye, K., & Tsoar, H. (2009) *Aeolian Sand and Sand Dunes*. Berlin. Heidelberg: Springer. DOI: 10.1007/978-3-540-85910-9.
- Schmidt, D. S., Schmidt, R. A., & Dent, J. D. (1998). Electrostatic Force on Saltating Sand. *Journal of Geophysical Research*, 103(8), 8997–9001.
- Stephen, H., & Long, D. G. (2005). Microwave Backscatter Modeling of Erg Surfaces in the Sahara Desert. *IEEE Trans. Geosci. and Rem. Sens.*, 43(2), 238–247.
- Stow, C. D. (1969). Dust and Sand Storm Electrification. *Weather*, 24(4), 134–137.
- Tajudin, M. T. J. (2014). *Study and design of reconfigurable antennas using plasma medium*. Universite Rennes 1. Retrieved from <https://tel.archives-ouvertes.fr/tel-01060295>.
- Williams, K. K., & Greeley, R. (2004). Laboratory and field measurements of the modification of radar backscatter by sand. *Remote Sensing of Environment*, 89, 29–40.
- Zolotokrylin, A. N. (2003). *Desertification climatique*. Moscow: Nauka.

#### МОДЕЛЮВАННЯ РАДІОЛОКАЦІЙНОГО РОЗСІЮВАННЯ ЕОЛОВИМИ ФОРМАМИ РЕЛЬЄФУ ПУСТЕЛЬ

О. Я. Матвеев, С. А. Величко, Д. М. Бичков, В. К. Иванов, В. М. Цимбал

Інститут радіофізики та електроніки ім. О. Я. Усикова НАН України, вул. Акад. Проскури, 12, Харків, 61085, Україна

З метою виявлення походження ефекту аномально вузькоспрямованого зворотного розсіювання радіохвиль (АВЗРР) СМ-діапазону у пустельних районах у статті описаний комплексний аналіз багаторічних досліджень ділянок пустелі Сахари. За результатами аналізу, який виконувався із застосуванням радіолокаційних даних РСА супутника “Envisat-1”, результатів контактних вимірів, погодних умов та з урахуванням сучасних теорій, виконано моделювання особливостей розсіювання радіохвиль еоловим рельєфом пустелі. Запропоновано нову модель аномального зворотного розсіювання, за якою головним розсіювачем у бік радіолокатора є решітка, що сформована вітром з наелектризованих сальтонів та рептонів на висоті 2–3 см від поверхні і повторює рельєф брижів та барханів. Нова модель дала змогу пояснити головні особливості експериментальних досліджень ефекту АВЗРР. А саме: залежність ефективної поверхні розсіювання радіохвиль досліджуванім рельєфом від швидкості приповерхневого вітру до 10 м/с при зустрічних напрямках векторів вітру і радіозондування поверхні, а також при їх взаємному азимутальному відхиленні на  $\pm 45$  град. За використанням нової моделі запропоновано супутниковий контроль вологості приповерхневого шару пустельних районів Землі на довжинах радіохвиль 3 см і 5.6 см з кутами огляду 30...35°.

**Ключові слова:** радіолокаційне дистанційне зондування, моніторинг пустелі, аномально вузькоспрямоване зворотне розсіювання, піщаний наелектризований шар.

Рукопис статті отримано 09.01.2023